Applied Catalysis B: Environmental 176–177 (2015) 699–708

Contents lists available at ScienceDirect

Applied Catalysis B: Environmental

journal homepage: www.elsevier.com/locate/apcatb

Preparation, characterization and NH_3–SCR activity of $FeVO_4$ supported on TiO_2–WO_3–SiO_2

Marzia Casanova [a], Luca Nodari [b], Amod Sagar [c], Karl Schermanz [c], Alessandro Trovarelli [a,*]

[a] Dipartimento di Chimica, Fisica e Ambiente, via del Cotonificio 108, Università di Udine, 33100 Udine, Italy
[b] Istituto per l'Energetica e le Interfasi – IENI – Consiglio Nazionale delle Ricerche, Corso Stati Uniti 4, 35127 Padova, Italy
[c] Treibacher Industrie AG, Division of Chemistry R&D, Auer von Welsbach Strasse 1, A-9330 Althofen, Austria

ARTICLE INFO

Article history:
Received 20 February 2015
Received in revised form 25 April 2015
Accepted 30 April 2015
Available online 2 May 2015

Keywords:
SCR
$FeVO_4$
Selective catalytic reduction
Iron vanadate
Mössbauer
TiO_2–WO_3–SiO_2

ABSTRACT

A series of $FeVO_4$ catalysts supported on TiO_2–WO_3–SiO_2 based oxides were prepared and studied in the ammonia SCR reaction. Their characteristics have been studied by X-ray powder diffraction, X-ray fluorescence, surface area measurements, Mössbauer spectroscopy and temperature programmed methods. It is shown that homogeneity of starting $FeVO_4$ powder is one of the parameters that governs the activity of the final catalytic material. Stoichiometric or Fe/V rich compositions can be obtained by varying the pH of precipitation; this affects interaction with the support and thermal stability, which in turn modifies SCR activity. Homogeneous $FeVO_4$ shows the highest activity and thermal stability which might be correlated with the characteristics of Fe^{3+}—O—V^{5+} bond and the acidity of the V—O moiety. Both vanadium and iron excess promote phase evolution of the support with formation of rutile and consequent surface area loss at much lower temperature.

1. Introduction

NH_3–SCR is one of the most reliable technologies for the removal of NO_x from both stationary and mobile applications. In particular, the applicability to automotive emission abatement requires the use of very efficient catalysts showing high NO_x conversion at the low temperature side of the activity window, high N_2 selectivity, good thermal stability and low environmental impact [1–5]. Two classes of catalyst formulations have been intensively investigated in the last decade: vanadium-free zeolite-based catalysts, like the new generation Cu–Zeolites, which can guarantee 95% NO_x removal even at very low temperatures [6–13] and vanadium-based catalysts, which have been successfully used in the deNO_x process for heavy duty diesel engines [14–17]. Vanadia applications are also of primary interest in developing countries and in some off-road applications, which require less demanding NO_x elimination standards [18].

The introduction of vanadium in SCR catalysts in the form of a vanadate as an alternative to V_2O_5 has been proved to be an effective method to face the main drawbacks of vanadia-based materials like the lack of sufficient thermal stability, catalytic activity performances and toxicity related to volatility [19–21]. In particular, we previously studied the effect of rare earth dopants in the V_2O_5/TiO_2–WO_3–SiO_2 system resulting in the formation of stable and SCR active rare earth vanadates; amongst the dopants, terbium and erbium were shown to be the most promising compositions in terms of activity and thermal stability [19,22]. Iron and other metal vanadates have also been reported recently to be a valid alternative to V_2O_5, showing excellent NO_x removal efficiency and good H_2O/SO_2 durability [23–25]. Other mixed transition metal/rare earth metal vanadates have been used as well, showing an improvement of activity and stability against traditional vanadia-based materials [26]. Specifically, the formation of mixed $Fe_{0.5}Er_{0.5}VO_4$, supported on TiO_2–WO_3–SiO_2 showed the optimal trade off between the low temperature activity and thermal stability required for mobile SCR applications [26]. This was due to the ability of Er to enhance the structural and textural stability of the material by hindering the transformation of anatase to rutile and by the promotion of low temperature activity due to the presence of Fe within the vanadate structure. In these studies, we showed that the introduction of $FeVO_4$ promoted low temperature activity by modifying the redox/acid–base properties; however this occurred with a loss in thermal stability, likely originating from the presence of traces of Fe_2O_3 or V_2O_5 which accelerates the anatase phase transition to rutile of the titania-based support and reaction between the various components of the

* Corresponding author. Tel.: +39 0432558855; fax.: +39 0432558803.
E-mail address: trovarelli@uniud.it (A. Trovarelli).

http://dx.doi.org/10.1016/j.apcatb.2015.04.056
0926-3373/

catalyst. In order to improve the stability of iron-based catalysts we have investigated here the effect of the catalyst preparation on a series of $FeVO_4$-based catalysts obtained by coprecipitation under different conditions. Selected compositions have been studied in detail by powder X-ray diffraction, Mössbauer spectroscopy and temperature programmed methods. The resulting catalysts showed different compositional homogeneity that can affect catalytic behaviour and thermal stability. The presence of iron and vanadium oxides together with the vanadate influences thermal stability; this aspect can be partially governed by the preparation method that guarantees the production of pure stoichiometric $FeVO_4$. The effect of loading of $FeVO_4$ on TiO_2–WO_3–SiO_2 was also investigated to optimize the catalytic behaviour.

2. Experimental

2.1. Materials and methods

For the preparation of $FeVO_4$ samples a solution of Fe(III) nitrate nonahydrate $Fe(NO_3)_3{\cdot}9H_2O$ (Treibacher) in deionized water was mixed under continuous stirring with a solution prepared by dissolving ammonium metavanadate NH_4VO_3 (Aldrich) in deionized water at approximately 80 °C. The pH of the mixture was then adjusted to a value between 1 and 9 by adding ammonia solution. The first sample at pH1 was prepared by mixing the two solutions without addition of ammonia. The precipitate was stirred, filtered, washed and dried. The resulting nine samples ($1 \leq pH \leq 9$) were characterized by powder X-ray diffraction, B.E.T. surface area measurements, Mössbauer spectroscopy and temperature programmed methods before mixing with the support.

For the preparation of the supported catalysts, the iron vanadate was used to prepare an aqueous slurry which was mixed with a second slurry containing the commercial support of composition 81% TiO_2–9% WO_3–10% SiO_2 (provided as commercial product "TIONA DT-58" from Cristal Global, indicated throughout the paper as TWS). The weight ratio of metal vanadate/TWS typically was 8.4/91.6, in agreement with our previous investigations [19,22,24], but a series of samples with varying $FeVO_4$ loading from 1 to 15 wt.% was also prepared. The combined slurries were evaporated to dryness and the solid obtained was dried at 120 °C followed by calcination at 650 °C for 2 h to yield the fresh catalyst powder. Aging treatments were carried out on the fresh catalyst in a muffle furnace at different temperatures in the range 700–750 °C for 10 h.

The surface areas of the catalysts were measured with the B.E.T. method by nitrogen adsorption at −196 °C, using a Tristar 3000 gas adsorption analyser (Micromeritics). X-ray powder diffraction patterns of the samples were collected in the range $10° < 2\theta < 60°$ using a Philips X'Pert diffractometer equipped with a Ni-filtered Cu Kα radiation operated at 40 kV and 40 mA. Phase identification was carried out using Philips X'Pert HighScore software.

TPR experiments were carried out in a TG apparatus (TA instruments Q500) using a catalyst sample loading of ca. 15 mg that was pretreated at 500 °C in flowing dry air for 1 h. After cooling under a Ar flow down to room temperature, the gas was switched to a 5% H_2/Ar gas mixture. The temperature was then increased from room temperature to 900 °C at a heating rate of 10 °C/min in the same gas mixture with a flow rate of 60 ml/min. Reduction was then calculated from derivative weight loss analysis.

X-ray fluorescence analysis were performed with an Epsilon 5 EDXRF spectrometer (Panalytical), which utilizes secondary excitation from 11 secondary selectable targets. The spectrometer employs a Gd X-ray tube operating at a maximum power of 600 W and voltage between 25 and 100 kV and a solid state germanium detector (PAN-32) with an energy range between 0.7 and 100 keV and a resolution <140 eV. Analysis on both liquid and loose powder samples were performed in He atmosphere; sample cups were equipped, respectively, with polypropylene and mylar films. All data were analysed with the Epsilon 5 software.

DTA measurements were performed in a combined TGA–DSC apparatus (TA instruments SDT Q600) using a catalyst sample loading of ca. 9 mg in an alumina crucible. Different experiments were conducted by heating the sample under air up to 800/1000 °C with a heating ramp of 10 °C/min.

Mössbauer spectroscopy was performed on a conventional constant acceleration spectrometer, with a room-temperature Rh matrix ^{57}Co source, nominal strength 1850 MBq. The spectra were collected at room temperature and when necessary at 20 K, using an ARS® close circuit cryostat. The hyperfine parameters isomer shift (δ), quadrupole splitting and/or quadrupole shift if magnetic coupling is present (Δ/e), linewidth at half maximum (Γ) were expressed in mm/s while the relative area (A) in %. The parameters were obtained by means of standard least-squares minimization techniques. The spectra were fitted to Lorentzian line shapes with the minimum number of doublets. δ is quoted to α-Fe. The hyperfine parameters are reported in Supplementary data section (Table S1).

2.2. Testing of catalysts in the NH_3–SCR reaction

NH_3–SCR activity studies were conducted by means of a laboratory equipment [26] under the conditions reported in Table 1. The powder catalyst was placed in a down-flow tubular quartz microreactor inserted in a furnace; the temperature was controlled by a thermocouple in contact with the catalytic bed. High space velocities were used in order to obtain conversions typically in the range 40–90%. Mass flow meters were used to measure and control the single gaseous streams, while water was added by using an injection pump. The feed stream was preheated and premixed with the exception of ammonia which was added to the gas mixture immediately before entering the microreactor in order to avoid side reactions. Activity of the samples was measured under stationary conditions in a temperature range of 200–500 °C. The gas composition after SCR reaction was analysed with an FT-IR spectrometer (MKS Multigas Analyzer 2030) equipped with a heated multi-pass gas cell (5.11 m length).

3. Results

3.1. Characterization of $FeVO_4$

Mixing of $Fe(NO_3)_3{\cdot}9H_2O$ and NH_4VO_3 solutions under the conditions reported in the experimental section causes the precipitation of $FeVO_4$ as a brown–yellowish powder. After separation of the precipitate, the light color of the remaining solutions indicates the presence of residual components from the precursor salts. The solutions obtained after filtration and the filtered powders

Table 1
Experimental conditions and feed gas composition for catalytic tests.

Catalyst weight	100 mg
Particle size	355–425 μm
Total flow	0.3 l/min
GHSV	180,000 h^{-1}
Temperature range	200–500 °C
Gas composition	
NO	200 ppm
NH_3	220 ppm
O_2	20,000 ppm
H_2O	10%
N_2	balance

Table 2
Fe/V ratio and surface area data of bare and supported $FeVO_4$.

B.E.T. surface area (m^2/g)						
pH	Fe/V ratio[a]	$FeVO_4$ dried	$FeVO_4$ 650 °C/2 h	$FeVO_4$/TWS 650 °C/2 h	$FeVO_4$/TWS 700 °C/10 h	$FeVO_4$/TWS 750 °C/10 h
1	0.888	12	2	71	29	4
2	0.947	23	6	73	31	4
3	0.993	37	8	74	31	4
4	1.000	46	8	75	34	5
5	1.000	47	8	77	36	5
6	1.000	47	8	76	35	5
7	1.027	60	8	77	35	5
8	1.028	67	8	75	23	5
9	1.048	78	1	73	20	4

[a] Atomic Fe/V ratio as calculated from powder x-ray fluorescence.

were analysed by means of XRF. The results obtained are shown in Fig. 1 and Table 2, respectively. Fig. 1 shows the concentration of vanadium and iron remaining in solution after precipitation. The samples can be divided into three groups: for $1 \leq pH \leq 3$ a decreasing concentration of V and Fe was detected in solution; Fe concentration, in this range, is higher than V, and the corresponding atomic Fe/V ratio in the powder material is lower than 1, indicating the presence of excess vanadium (Table 2). For $4 \leq pH \leq 6$, neither vanadium nor iron were found in the solutions, while at pH higher than 6 only vanadium was detected with concentration increasing progressively with pH. In summary, it is found that only for an intermediate pH range a stoichiometric Fe/V ratio is found on the final material. Consequently we used the composition prepared at pH5 as representative of stoichiometric $FeVO_4$, hereinafter indicated as $FeVO_4$/pH5.

Surface area results of all samples are also reported in Table 2. For the dried vanadates surface area increases with pH values from 12 m^2/g (pH1) up to 78 m^2/g (pH9). A significant decrease was observed after aging at 650 °C/2 h for all samples with a drop to values in the range 1–8 m^2/g.

All the dried samples were amorphous to XRD; by increasing the calcination temperature from 650 °C to 800 °C the patterns show sharp and well defined peaks which indicate the formation of crystalline $FeVO_4$ (Fig. 2). The main diffraction peaks were observed at $2\theta = 24.90, 27.17$ and 27.55 corresponding to diffraction of (120), $(0\bar{1}2)$ and $(\bar{2}20)$ lattice planes of triclinic iron orthovanadate (JCPDS 38-1372), which is the only crystalline component identified in all samples. The only exception was the sample made at pH1 aged at 650 °C/2 h that showed the presence of two different crystalline phases identified as two different forms of iron vanadate; i.e. the orthovanadate $FeVO_4$ and the tetrapolyvanadate $Fe_2V_4O_{13}$ which disappeared after thermal treatment at 750 °C/10 h. None of these samples showed the presence of macrocristalline hematite.

Treatment at temperature exceeding 800 °C causes decomposition of $FeVO_4$ with segregation of V_2O_5 due to the melting of iron vanadate taking place at 860 °C [27]. Phase stability and thermal profile behaviour was checked on stoichiometric $FeVO_4$/pH5,

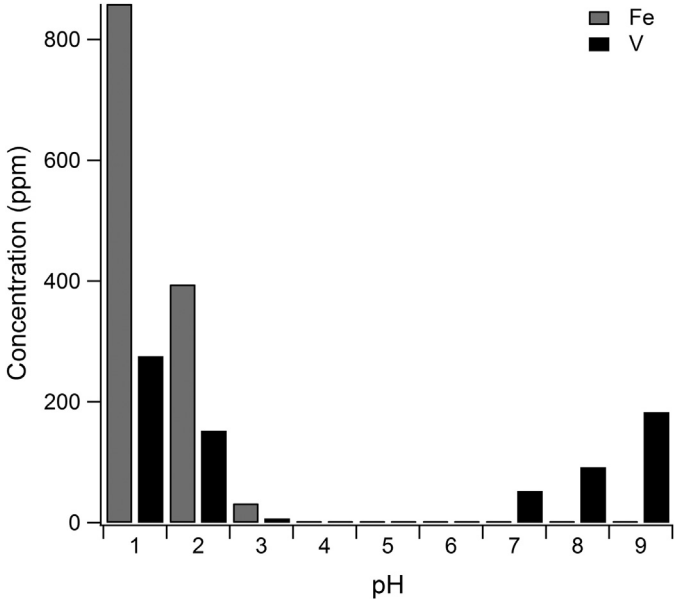

Fig. 1. XRF of solutions after precipitation of $FeVO_4$ at pH values 1–9.

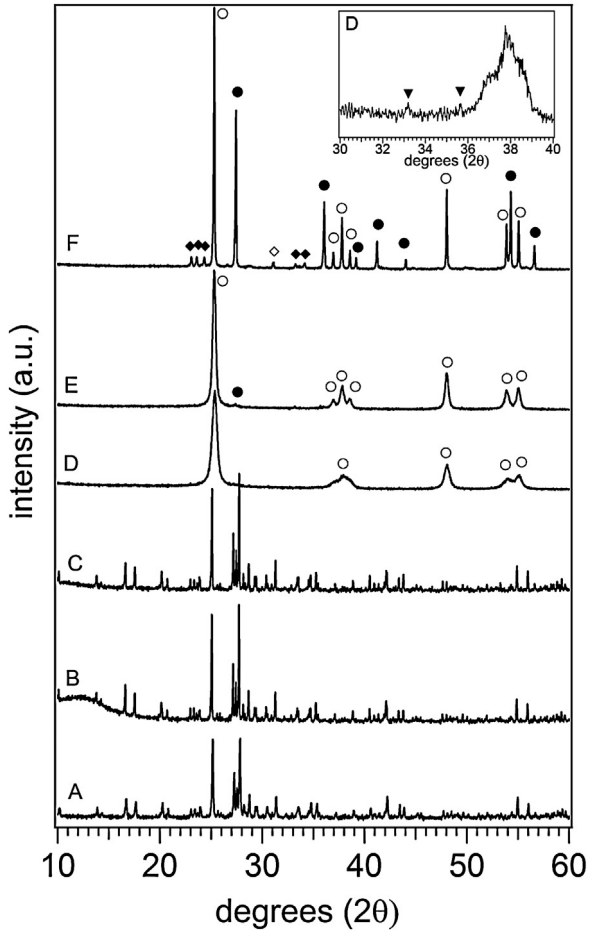

Fig. 2. XRD patterns of $FeVO_4$/pH5 after aging at 650 °C/2 h (A), 750 °C/10 h (B) and 800 °C/10 h (C), and $FeVO_4$/pH5/TWS aged at 650 °C/2 h (D), 700 °C/10 h (E) and 750 °C/10 h (F). TiO_2 anatase (○), TiO_2 rutile (●), WO_3(♦), Fe_2WO_6 (◊), hematite (Fe_2O_3) (▼). In the inset a magnification of spectrum D is shown in the 2θ range 30–40° where peaks due to hematite are indicated.

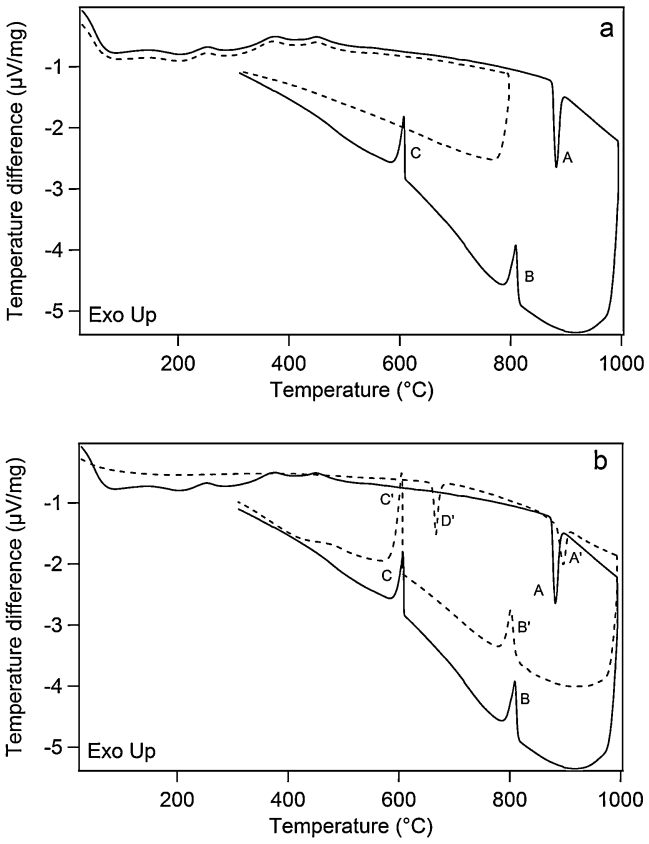

Fig. 3. (a) DTA (heating and cooling cycle) of $FeVO_4$/pH5 from room temperature to 800 °C (--------) and from room temperature to 1000 °C (----). (b) DTA (heating and cooling cycle) of $FeVO_4$/pH5 from room temperature to 1000 °C: first (----) and second (--------) cycle. (A) endothermic peak due to $FeVO_4$ melting, (B) exothermic peak due to re-crystallization of $FeVO_4$, (C) exothermic peak due to V_2O_5 crystallization, (D) endothermic peak due to V_2O_5 melting.

as representative sample, by TG/DTA heating the sample from room temperature up to 1000 °C. A strong endothermic peak is observed around the melting temperature of the vanadate (signal A in Fig. 3a); upon cooling two exothermics appeared (B and C), one corresponding to the re-crystallization of part of the vanadate (B) and the second corresponding to the crystallization of V_2O_5 (C) which was identified by XRD analysis (see Fig. S1). $FeVO_4$ melts incongruently with deposition of α-Fe_2O_3 at the temperature of 860 °C and as a consequence hematite is not affected by the thermal treatment [28]. To confirm that only thermal treatments at temperatures exceeding the decomposition point of the vanadate generated free-V_2O_5, an additional experiment was performed heating the sample up to 800 °C. The result is shown by the dotted line in Fig. 3a, where no signals corresponding to crystallites of V_2O_5 were detected. A second DTA cycle was performed after cooling the sample recovered from the first cycle up to 1000 °C (Fig. 3b). During the second heating ramp up to 1000 °C an additional endothermic signal appeared at the temperature of 650 °C (signal D′) which can be attributed to the melting of V_2O_5. This indicates that part of the sample is already in the form of vanadium oxide from the beginning of the second cycle; this V_2O_5 originates from decomposition of the vanadate in the first heating ramp. For this reason the $FeVO_4$ decomposition peak is less intense in the second heating cycle (compare signal A and A′), while, during the cooling ramp, the crystallization peak of V_2O_5 is more intense (compare signal C and C′).

In order to further investigate the structural features of $FeVO_4$ Mössbauer spectroscopy analysis was carried out on two selected samples ($FeVO_4$/pH5 and $FeVO_4$/pH9) in the dried state and after the thermal treatment at 750 °C/10 h. The reason for selecting these two candidates was to investigate the compositional homogeneity of a stoichiometric sample ($FeVO_4$/pH5) and a sample with a slight excess of iron ($FeVO_4$/pH9). The RT Mössbauer spectrum of dried $FeVO_4$/pH9 exhibited an intense, slightly asymmetric, doublet centred at about 0.35 mm/s. The centre shift is compatible with the presence of Fe(III) and the best fitting was obtained by a 3 components model. The outer doublet, which exhibits the highest Δ (1.26 mm/s), can be attributed to pentacoordinate Fe(III) (site A, red line in Fig. 4a), the other two to Fe(III) in octahedral site (sites B and C blue lines, Fig. 4a). The high Δ value in site A, representative of the high distortion of a pentacoordinate site, is compatible with a trigonal bypiramidal site. The presence of a pentacoordinate site is supported by the structure expected for the Fe(III) orthovanadate [29,30]. Concerning the two octahedral sites, they differ both for distortion (Δ equal to 0.49 and 0.85 mm/s, respectively) and for site population (39% and 30%, respectively). The ratio amongst the relative areas of the three Fe sites is slightly different from the one expected for pure crystalline Fe(III) vanadate (i.e. 1:1:1) [31]. The ratio calculated from the relative areas, that is site A: site B: site C, is 1:1.8:1.9. These differences in site population can be ascribed to the low crystallinity of the sample [31], and/or to different recoilless fraction, *f*, of the three ferric species.

It is important to point out, that RT spectrum does not show any evidence of magnetic pattern, due to macrocrystalline magnetically coupled oxides, such as hematite. Also the 20 K spectrum does not show any sextets attributable to magnetically coupled species.

The Mössbauer analysis of $FeVO_4$/pH9 aged at 750 °C/10 h showed the contemporary presence of macrocrystalline hematite together with $FeVO_4$. In fact, the spectrum of the aged sample shows, beside the central absorption, the presence of a magnetic pattern, (Fig. 4b) with hyperfine parameters that can be ascribed to hematite [32]. The absence of signals due to hematite in the powder XRD profiles of $FeVO_4$/pH9 aged at 750 °C can be due to the lower specific sensitivity of X-ray to Fe containing species and to the absence of a sufficient degree of crystallinity of the Fe_2O_3 particles. As for the dried $FeVO_4$/pH9, the intense central absorption was fitted with three doublets, one due to pentacoordinate Fe(III) and two due to octahedral Fe(III) sites. It is worthy to note that the thermal treatments seem to affect also the site geometry by promoting a decrease in Δ (1.15 mm/s, 0.26 mm/s, 0.63 mm/s, respectively, for site A–C). Concerning the relative areas, the population of the magnetically split component is about 26% of the total amount of Fe, while the ratio between bypiramidal trigonal and the two octahedral sites is close to 1:1:1, within the experimental error.

Mössbauer spectra of $FeVO_4$/pH5 are close to those of $FeVO_4$/pH9 (Fig. 4c–d). The main difference is the absence of magnetically split components in the aged sample that confirmed the absence of hematite. Dried and aged $FeVO_4$/pH5 were fitted by using three doublets, the one with the highest Δ is attributable to pentacoordinate Fe(III), the other two to esacoordiante Fe(III). As for $FeVO_4$/pH9, the thermal treatment promotes a decrease in Δ, as a consequence of a decrease in site distortion. Vice versa, the relative area ratio seems to be less affected by thermal aging. Fresh and aged samples in fact, show similar relative area ratio (1:1.2:1.2, and 1:1.2:1, respectively, very close to the theoretical value, considering the experimental error), suggesting that the thermal treatment does not change substantially the Fe distribution over the three crystallographic sites.

The redox properties of $FeVO_4$ were also investigated by means of TPR experiments (Fig. 5). The reduction profile of $FeVO_4$ showed a broad main reduction peak in the range from 600 °C to 700 °C and from 700 °C to 850 °C for samples prepared at the lowest pH. Combining XRD data collected ex-situ during TPR (see Fig. S2) we can identify as reaction intermediates in the range of temperature

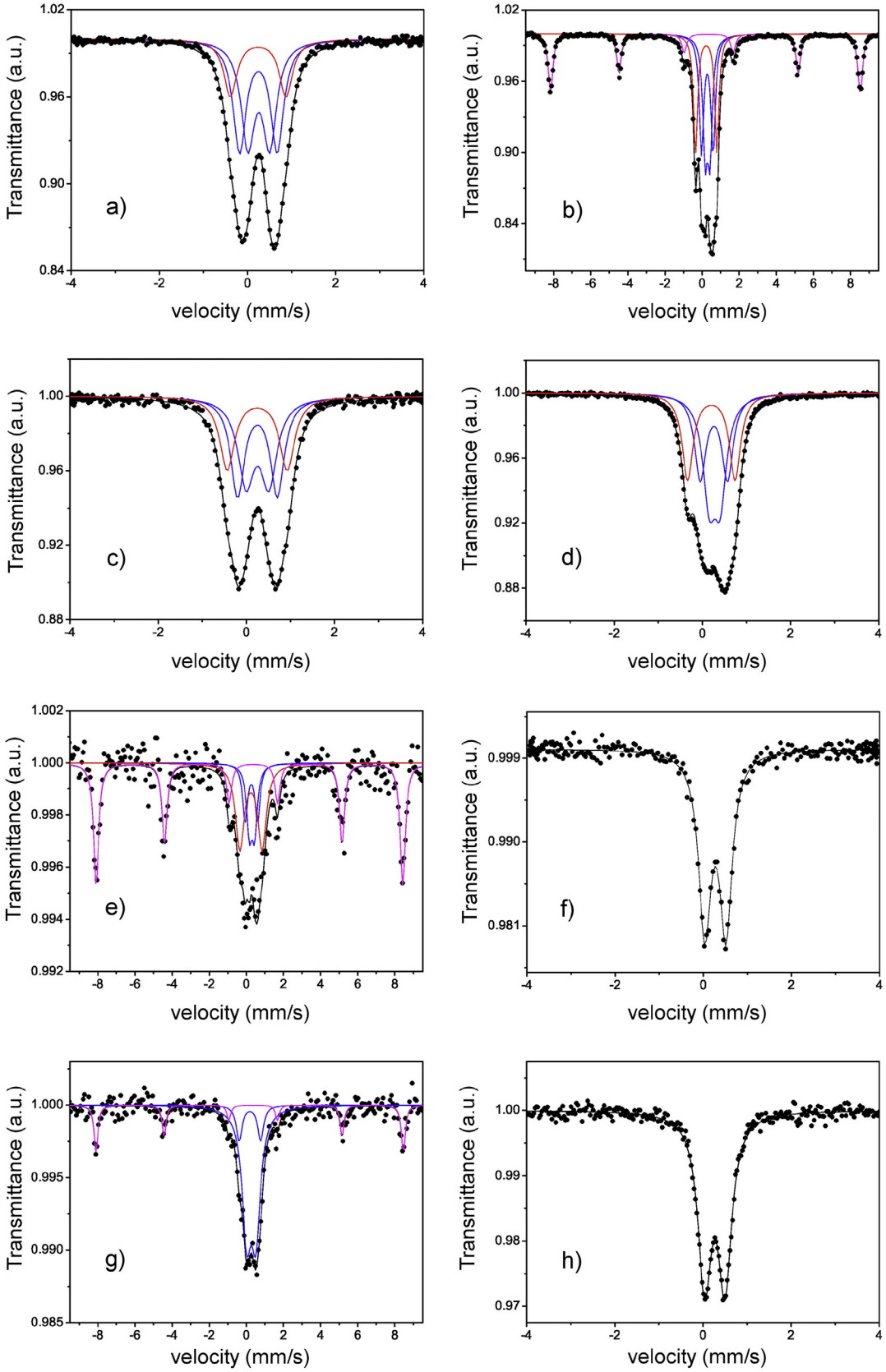

Fig. 4. Mössbauer spectra of $FeVO_4$/pH9 in fresh state (a) and aged at 750 °C/10 h (b); $FeVO_4$/pH5 in fresh state (c) and aged at 750 °C/10 h (d); $FeVO_4$/pH9/TWS aged at 650 °C/2 h (e) and at 750 °C/10 h (f); $FeVO_4$/pH5/TWS aged at 650 °C/2 h (g) and at 750 °C/10 h (h).

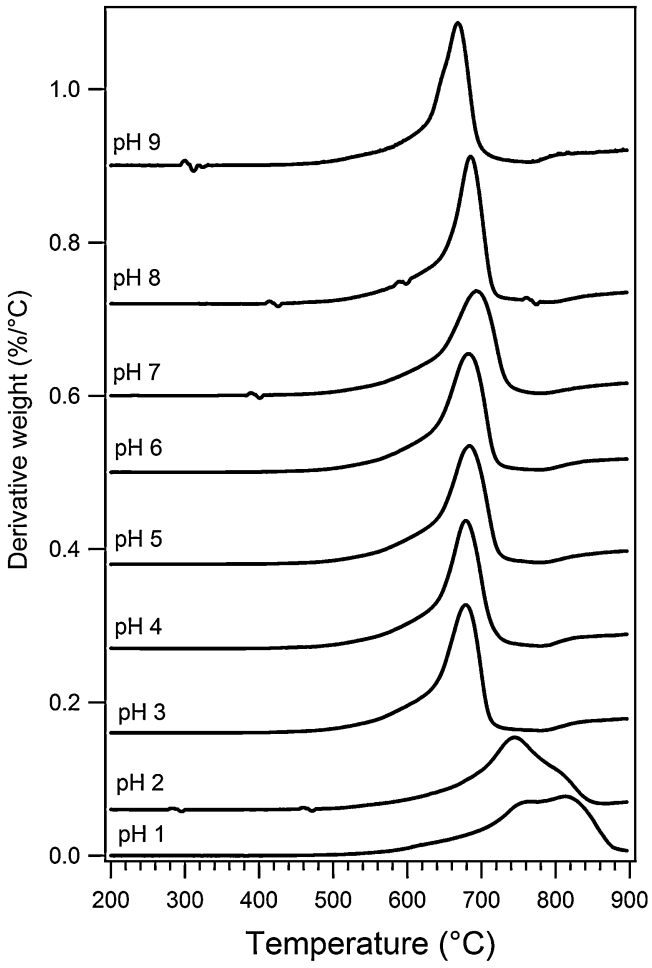

Fig. 5. Temperature programmed reduction of $FeVO_4$ derived from precipitation at different pH. Before TPR, samples were aged @650 °C/2 h.

from 500° to 600 °C either FeV_2O_4 and Fe_2O_3 or V_2O_3. At the higher temperature Fe_3O_4 is detected as final product with weak signals belonging to V_2O_3.

Quantitative evaluation of H_2 consumption ranges between 7.53 and 8.12 mmol of H_2 per gram of catalyst, which is in good agreement with the following decomposition/reduction pathway:

$$6FeVO_4 \rightarrow 2Fe_3O_4 + 3V_2O_3 + 7H_2O \quad (1)$$

Alternative decomposition pathways, like those reported in [29] are likely to be operative at lower temperature where reduction of Fe(III) to magnetite is still not complete.

3.2. *Characterization of $FeVO_4$ supported on TiO_2–WO_3–SiO_2*

B.E.T. surface area values of supported catalysts are reported in Table 2. For the fresh materials the surface area values are in the range 71–77 m^2/g. Aging at 700 °C/10 h causes a surface area loss higher than 50%, the samples prepared at pH 8–9 showing the most remarkable drop to 20–23 m^2/g. Further aging at 750 °C/10 h induces a major surface area drop with final values in the range 4–5 m^2/g.

Structural XRD data of the stoichiometric composition ($FeVO_4$/pH5) supported on TWS are shown in Fig. 2 (profiles D–F). For the fresh catalyst, anatase was the only phase detected with the main peak at ca. 25°. Diffraction lines belonging to Fe vanadate cannot be detected due to its low degree of crystallinity. Weak signals originating from Fe_2O_3 are also distinguished at ca. 33–36° (see inset of Fig. 2) indicating that interaction between the active phase and the support promotes a minor decomposition of $FeVO_4$ to Fe_2O_3. The corresponding vanadium is expected to form V_2O_5, which is difficult to detect by XRD at low concentration [33]. Furthermore it is known that V_2O_5 may not be present as an oxide on the surface of TiO_2 but may form different types of vanadates (mono-, di- and polyvanadates) when in contact with the surface of TiO_2 [34]. After aging at temperatures higher than 700 °C the diffraction profiles show the development of peaks originating from the modification of the support. In particular the transformation of TiO_2 anatase to rutile is evidenced from the appearance of rutile peaks and segregation of WO_3. In addition, peaks corresponding to Fe_2WO_6 were also observed indicating a reaction between Fe_2O_3 and WO_3. A similar behaviour, characterized by anatase to rutile transformation at high temperatures, was observed for all $FeVO_4$ samples. Generally, TiO_2 phase transformation is enhanced by the presence of V_2O_5 with the intensity of the rutile diffraction line being stronger than that of the anatase phase. This is true for the samples prepared at the lowest pH values (see Fig. S3, A). At higher pH values (pH ≥ 6), on the samples containing Fe_2O_3, the rutile formation is partly hindered. All XRD profiles show diffraction lines attributable to Fe_2WO_6 (see Fig. S3, B).

Mössbauer analysis was carried out on two representative samples of supported $FeVO_4$ ($FeVO_4$(pH5)/TWS and $FeVO_4$(pH9)/TWS) in the fresh state and after aging at 750 °C for 10 h. In both cases the presence of hematite was detected, indicating that interaction of $FeVO_4$ with the support enhances the partial decomposition of $FeVO_4$ with formation of Fe_2O_3. As above mentioned, the Mössbauer spectrum of the fresh supported $FeVO_4$/pH9 is characterized by a magnetic component and a Fe(III) paramagnetic absorption (Fig. 4e). It is worthy to note that this spectrum exhibits an absorption considerably lower than the unsupported sample, under similar experimental conditions, due to the lower loading of Fe in this sample. As for $FeVO_4$/pH9 the best fitting was obtained by using four components: a sextet, which can be attributed to hematite, and three doublets. The one with highest Δ, due to the presence of pentacoordinate Fe(III) in trigonal bypiramidal site (site A), the others attributed to hexacoordinate Fe(III) in octahedral sites (sites B and C). Concerning the sites population, Fe is distributed for the 48% over the magnetically coupled component and for the 52% over the paramagnetic components. The intensity area ratio amongst the different ferric sites is quite far from the theoretical value (1:0.5:0.4 instead of 1:1:1); the population of site A is increased approximately twofold in comparison with the octahedral sites population. This high deviation from the theoretical value, can be due to low crystallinity and substoichiometry of the sample, as for $FeVO_4$/pH9. This evidence could also suggest a superimposition of two ferric doublets with similar hyperfine parameters.

The spectrum of $FeVO_4$(pH5)/TWS shows also the coexistence of a magnetic and a paramagnetic coupled component. The above model does not fit properly, without using constraints, with this sample; the best fitting was obtained by using three components, one for the magnetic pattern and two for the paramagnetic absorption. Concerning the magnetic component, the sextet hyperfine parameters are compatible with those of hematite, while the two doublets could be representative of Fe(III) in octahedral sites. In contrast to $FeVO_4$/pH9, it is not possible to discriminate between bypyramidal and octahedral site and, again, it can be related to the absence of a well crystallized $FeVO_4$, as underlined by XRD.

Differing from the aged $FeVO_4$/pH5 and $FeVO_4$/pH9, the Mössbauer spectra of the supported samples thermally treated at 750 °C/10 h are characterized by an intense doublet centred around 0.3 mm/s (Fig. 4g-h). No magnetic component attributable to hematite was detected, both in the RT and in the 20 K spectra. The best fit was obtained by a single Fe(III) hexacoordinate component. Fe(III) in octahedral site is compatible with the presence of Fe_2WO_6

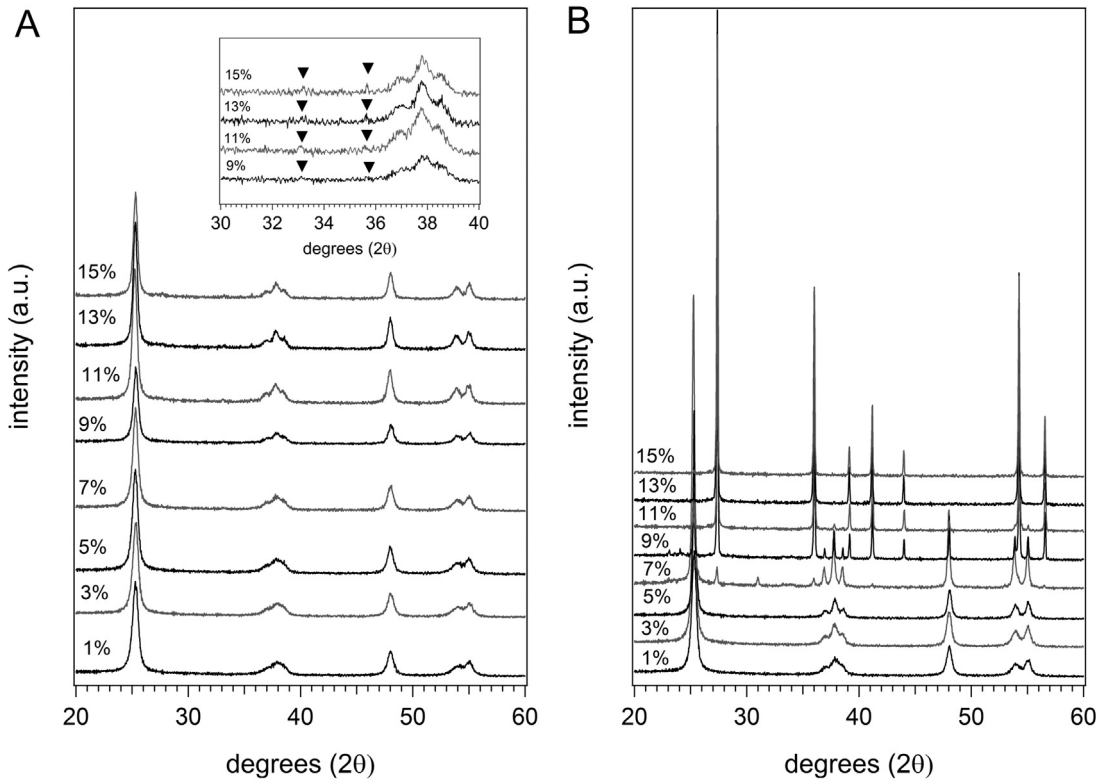

Fig. 6. XRD profiles of (1–15 wt.%)$FeVO_4$/pH5/TWS after aging at 650 °C/2 h (A) and after aging at 700 °C/10 h (B).

[35], identified also by XRD. This indicates that hematite reacts with WO_3 segregated from the support at these temperatures in agreement with results from XRD profiles that do not show the presence of Fe_2O_3 at the highest temperature (see profiles E and F in Fig. 2).

A series of $FeVO_4$/TWS samples at increasing $FeVO_4$ loadings, starting from stoichiometric pure $FeVO_4$/pH5, were also prepared and characterized for testing in SCR reaction. As can be seen from Fig. 6A, X-ray diffraction profiles of samples treated at 650 °C/2 h show only peaks belonging to anatase; only in the samples with a $FeVO_4$ loading in the range 9–15 wt.% Fe_2O_3 diffraction lines appear.

Fig. 6B shows that high temperature treatments (e.g. 700 °C) represent critical conditions leading to phase transition of the titania component of the support and modification of textural properties. Higher $FeVO_4$ loadings promote faster anatase to rutile transformation with associated formation of Fe_2WO_6. Rutile appears in the spectrum of the sample with a $FeVO_4$ loading of 7 wt.%. The subsequent spectra (9–15 wt.%) show intense diffraction lines due to rutile. This transformation is also confirmed by surface area properties (Fig. 7) which at higher temperature are strongly dependent on the amount of $FeVO_4$ loading.

3.3. NH_3–SCR activity

Detailed information about catalytic activity of supported $FeVO_4$/pH5 is given in Fig. 8 where NO conversion efficiencies and N_2 selectivity of fresh and aged samples in the 200–500 °C temperature range are reported. The activity profile in the so called fresh state resembles those observed in SCR reaction with a typical volcano-type shape. The activity increases with increasing reaction temperature up to ca. 330–380 °C where a maximum NO reduction activity is observed; at this point the activity starts to decrease due to ammonia oxidation reaction to N_2O and NO, which is prevailing over its reaction to N_2. N_2 selectivity slightly decreases above 400 °C. The NO conversion profile of the sample aged at 700 °C/10 h is similar to the one of the fresh sample up to 400 °C, after which a remarkable loss of activity is observed. A further severe thermal treatment at 750 °C/10 h is detrimental for NO removal efficiency which drops dramatically with a maximum of 40% at 380 °C.

A better detail on the effect of different thermal treatments on all compositions investigated is given in Fig. 9 that shows NO_x conversion in the low (200–270 °C) and high (420–500 °C) temperature SCR window after increasing the severity of aging conditions. For fresh catalysts (aging at 650 °C/2 h) the activity in the low temperature range is not dependent on preparation conditions and it increases with temperature from 20% at 200 °C to 80% at 270 °C.

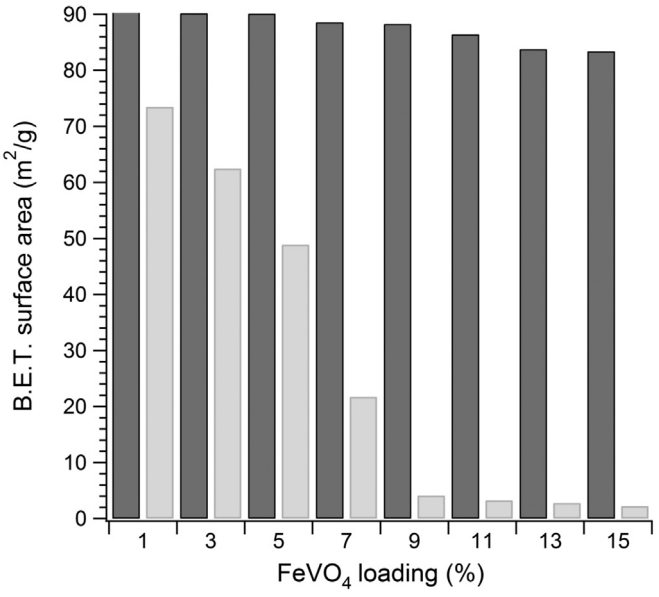

Fig. 7. B.E.T. surface area of (1–15 wt.%)$FeVO_4$/pH5/TWS after aging at 650 °C/2 h (dark gray) and after aging at 700 °C/10 h (light gray).

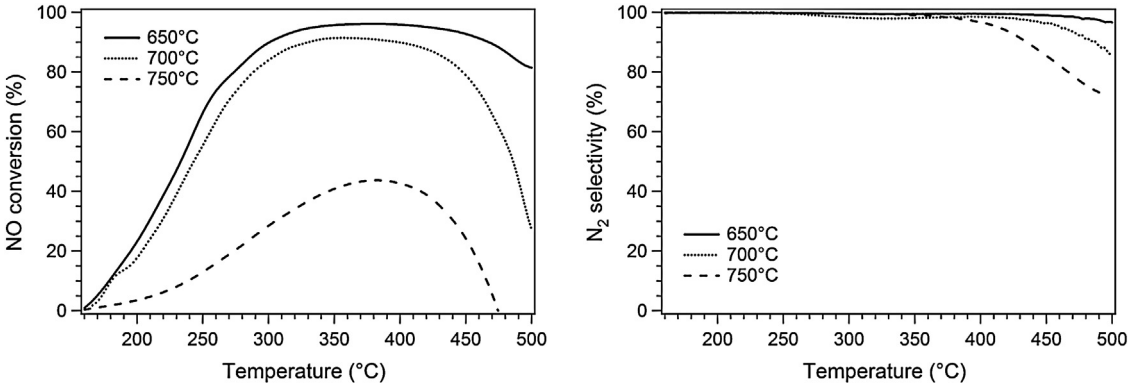

Fig. 8. NH_3–SCR activity and selectivity of $FeVO_4$/pH5/TWS.

In the high temperature range, conversions higher than 80% are observed with all samples excluding $FeVO_4$ prepared at pH9, where a little drop in activity is detected. The values of maximum NO conversion after aging at 700 °C show a marked influence of pH for all the SCR reaction temperatures. Better conversion performances are measured for samples prepared at pH ≥ 4 while at low pH a more severe drop of activity is observed in the high reaction temperature range.

At the most severe aging temperature (750 °C/10 h) the conversion drops in all samples to very low values; only samples prepared in the middle pH range still show a measurable NO reduction efficiency. From the above results it is clear that the control of the pH value of sample preparation is an important step, affecting the overall performances of supported $FeVO_4$ and its thermal stability. On the whole, preparation of vanadates at intermediate pH range ($4 \leq pH \leq 6$) can guarantee the best results in terms of activity and thermal stability which can be associated to the lower tendency of these compositions to promote dissociation of $FeVO_4$ to free iron and vanadium oxides.

Fig. 10 summarizes the behaviour of $FeVO_4$/pH5 supported on TWS at increasing $FeVO_4$ loading in the range of temperature 200–500 °C in the fresh state and after aging at 700 °C/10 h. The intensity of the brown colour clearly identifies the regions of higher conversion. For fresh catalysts the activity increases with $FeVO_4$ loading up to ca. 11 wt.% of catalyst. No further increase of activity is observed at higher loadings. After aging a marked shift of

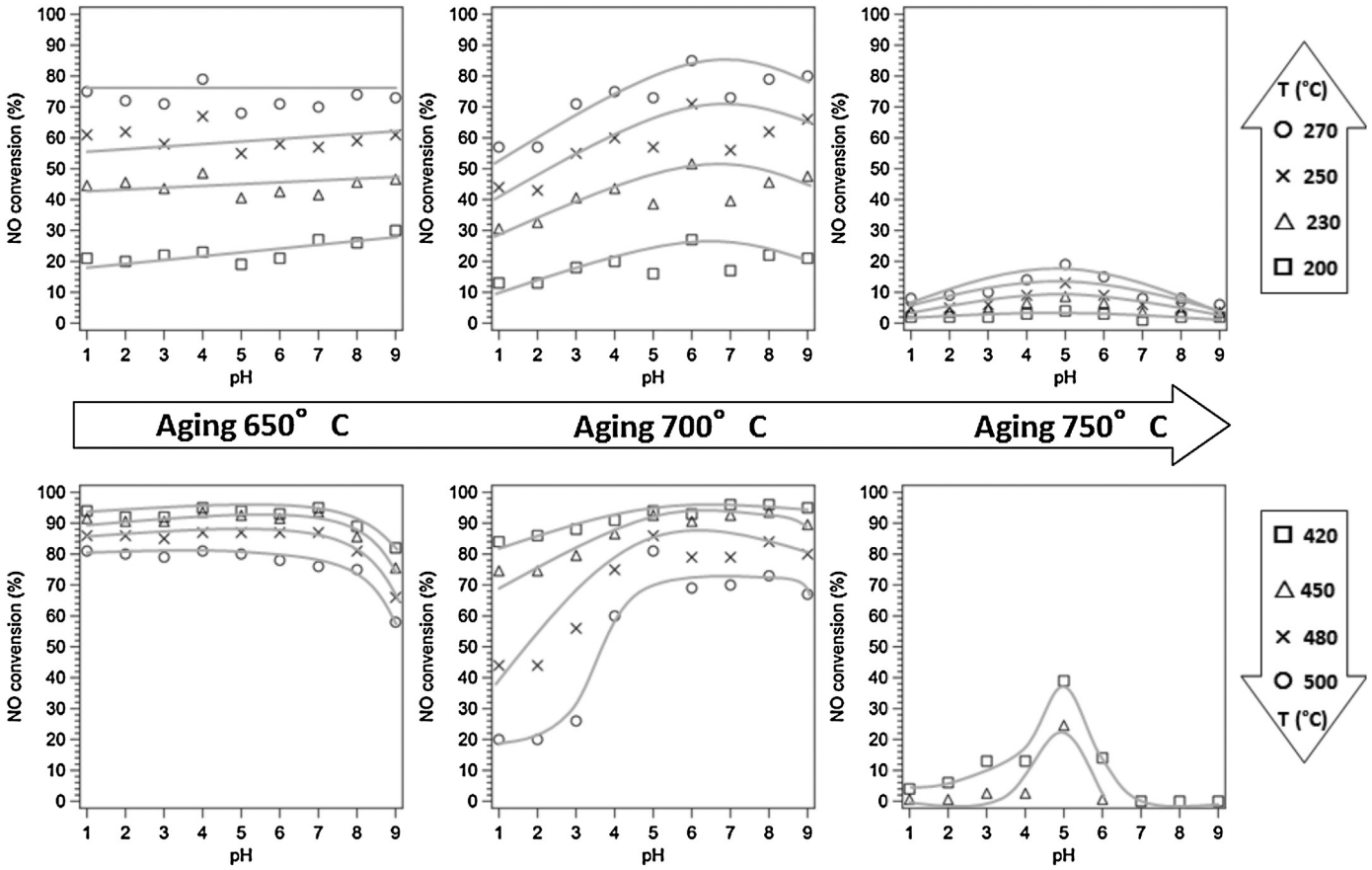

Fig. 9. Detail of catalytic activity of $FeVO_4$/pH1–9/TWS catalysts after increasing aging temperatures in the range 650–750 °C. Top: NO conversion curves in the low temperature portion of the SCR window (200–270 °C), Bottom: NO conversion curves in the high temperature portion of the SCR window (420–500 °C).

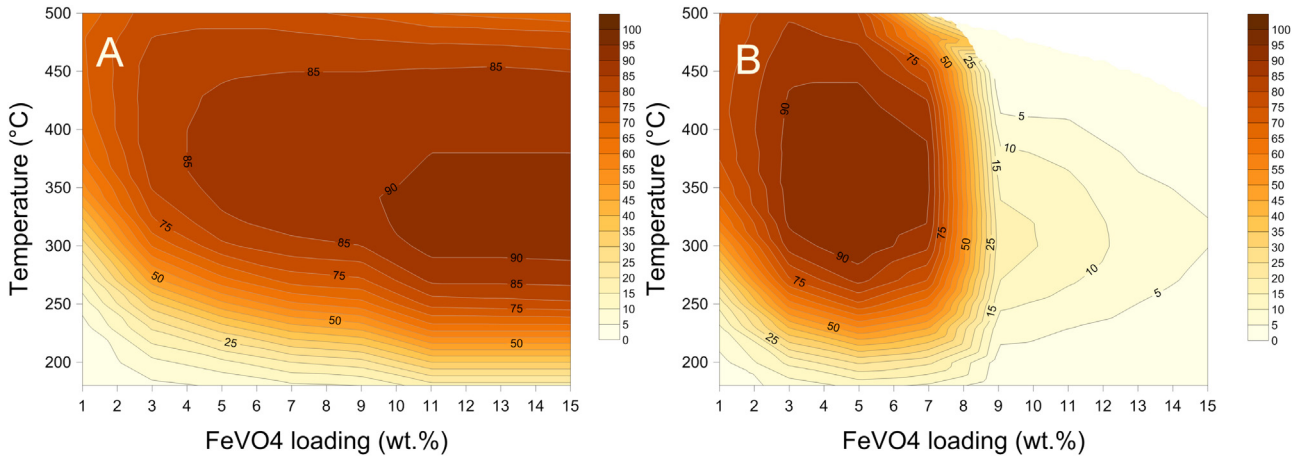

Fig. 10. Catalytic activity (NO conversion, %) of fresh (1–15 wt.%)$FeVO_4$/pH5/TWS (A) and after aging at 700 °C/10 h (B).

the high conversion region is observed in favour of catalysts with lower $FeVO_4$ loading; the best NO_x removal efficiency is shown at 5 wt.% loading and it rapidly decreases with increasing vanadate content. For loadings higher than 9 wt.% the activity is negligible in all the temperature range.

4. Discussion

We have recently found that the introduction of Fe in the form of a mixed iron–erbium vanadate confers to the catalyst formulation a higher SCR activity compared to compositions based on erbium vanadate only [26]. In particular the incorporation of Fe into $ErVO_4$ strongly improves the activity at the expenses of a limited loss in stability. The higher activity of $FeVO_4$/TWS and $Fe_xEr_{1-x}VO_4$/TWS compared to $ErVO_4$/TWS were associated to the modification of their redox/acid-base properties. However, the introduction of iron in the catalyst formulation reduces material stability towards rutilization, a process that is promoted by the presence of free vanadia on the catalyst surface. This, in turn, depends on the homogeneity and stability of iron vanadate. In the present study we have shown that the preparation of $FeVO_4$, by changing the pH of precipitation, influences homogeneity of the material. Stoichiometric $FeVO_4$ is found only if precipitation is carried out in the intermediate pH range ($4 \leq pH \leq 6$) while the presence of excess vanadium or iron is observed at lower and higher pH, respectively. This influences the properties of $FeVO_4$/TWS because excess iron/vanadium can affect the stability and activity of the active phase. The catalytic activity of the fresh catalysts (aged at 650 °C/2 h) is relatively independent of the pH of preparation (activity increases only slightly with pH at the lowest temperatures) with the exception of sample $FeVO_4$/pH9 that shows lower activity in the high temperature range. This sample is characterized by the highest Fe/V ratio (see Table 1) and the excess of Fe_2O_3 leads to a moderate deactivation compared to the homologous samples made at lower pH. Increasing the aging temperature to 700 °C causes a decrease of activity which is particularly significant for samples made at the lower pH range. The situation further changes with thermal treatment at 750 °C for 10 h which causes a severe drop in activity of all samples.

It is clear from XRD and Mössbauer analysis that supporting either stoichiometric or non stoichiometric $FeVO_4$ on TWS a fraction of Fe transforms into Fe_2O_3. This fraction is lower for samples prepared in the intermediate pH range and higher for the other. Semiquantitative evaluation from Mössbauer spectra reveals that in the stoichiometric catalysts 24% of iron exists as Fe_2O_3 on anatase support. At higher temperature Fe_2O_3 reacts with the tungsten fraction segregated from the support to give Fe_2WO_6. This reaction is not observed if bare Fe_2O_3 is supported on TWS (see Fig. S4); segregation of WO_3 from the support is in fact promoted by anatase-rutile transformation which in turn requires the presence of free vanadium oxide [36–37]. This result confirms that the iron vanadate, even if it is stable up to 800 °C, interacts with TWS support at lower temperatures. During this step, part of the iron moves out of the pentacoordinate site of the vanadate with the consequent release of free vanadium which acts then as a catalyst for the anatase to rutile transformation. Rutilization of TiO_2 with the resulting surface area drop causes the dramatic decrease of activity observed after aging at 750 °C.

Thermal stability and NH_3–SCR activity of the final catalyst are also influenced by the $FeVO_4$ loading. At the highest loading (up to 15 wt.%) formation of Fe_2O_3 can be detected by XRD (see Fig. 7); transformation of anatase to rutile becomes significant at loading higher than 7 wt.%. The effect of loading of $FeVO_4$ on TiO_2 support was also investigated by Liu et al. [23] who reported the enrichment of surface VO_x species on increasing coverage of $FeVO_4$. Since they did not observe presence of Fe_2O_3 by XRD, they considered this VO_x enrichment a purely surface process not affecting the bulk structure of $FeVO_4$ and positively influencing catalytic activity. At the same time, however, they observed loss of activity after aging which was attributed to the formation of rutile. Segregation of surface VO_x species was also observed on pure $FeVO_4$ in methanol oxidation reaction [38]. It is likely that segregation of vanadium is the consequence of either small deviation from stoichiometry in $FeVO_4$ or of the enhanced VO_x mobility associated to its lower Tammann temperature. This phenomenon is more evident at lower temperatures when $FeVO_4$ is supported on TWS. In this case a fraction of free iron oxide is detected already at 650 °C, indicating the presence of the corresponding amount of free VO_x. Weak signals characteristic of the presence of VO_x moieties can be detected by Raman spectroscopy and are attributable to deformation modes of V=O and V=O···V bonds [39] (Fig. S5), suggesting that part of the vanadate decomposes to surface vanadium containing species, as pointed out recently by Wu et al. [25]. These species could act as the true catalyst for NH_3–SCR reaction mediated by the presence of bulk $FeVO_4$ and Fe_2O_3 that are responsible for the better performance of these catalysts compared to V_2O_5 only materials [26]. The presence of Fe can act either by altering the electron density of VO_x surface species and particularly of V—O bond characteristics, and increasing also the Lewis acidity of the vanadium species. The importance of electronic effects between Fe^{3+} and V^{5+} in promoting SCR reaction has been also pointed out recently [23].

5. Conclusions

The control of the pH value during the synthesis of iron vanadate has been shown to be an effective way to govern the homogeneity of the final composition. Samples prepared at pH < 4 were rich in vanadium while stoichiometric $FeVO_4$ were obtained in the range $4 \leq pH \leq 6$; Fe_2O_3-rich samples characterize precipitation at pH higher than 6.

The situation changes considerably after supporting the vanadate on TiO_2–WO_3–SiO_2 as a strong interaction takes place between the two components of the catalyst. This interaction was evidenced by the formation of Fe_2WO_6 and rutile after thermal treatments. Deactivation of 8.4 wt.%$FeVO_4$/TiO_2–WO_3–SiO_2 SCR-catalysts is promoted by the presence of free vanadium species on the catalyst surface, which act as a catalyst in the anatase transformation into rutile and, consequently, promoting WO_3 segregation from the support with surface area drop and loss of activity. However, the composition of the starting $FeVO_4$ is still important in the development of the final SCR catalyst. Characterization of the supported samples highlighted the different behaviour of the Fe/V-rich samples against stoichiometric compositions towards rutile formation and its effect on catalytic activity. Catalysts derived from stoichiometric $FeVO_4$ showed the best compromise between catalytic activity and thermal stability.

Acknowledgments

The authors are grateful to Italy-Austria Interreg IV project Mat4Cata for financial support and to the Department of Chemical Science, University of Padua, for the use of Mössbauer Spectroscopy apparatus. We thank Dr. Alfonsina Pappacena from University of Udine for X.R.F. measurements and Dr. Francesco Puzzo from University of Bologna for Raman measurements.

Appendix A. Supplementary data

Supplementary data associated with this article can be found, in the online version, at http://dx.doi.org/10.1016/j.apcatb.2015.04.056.

References

[1] T.V. Johnson, SAE Int. J. Engines 5 (2012) 216–234.
[2] S. Roy, M.S. Hegde, G. Madras, Appl. Energy 86 (2009) 2283–2297.
[3] M. Weibel, N. Waldbüßer, R. Wunsch, D. Chatterjee, B. Bandl-Konrad, B. Krutzsch, Top. Catal. 52 (2009) 1702–1708.
[4] G.A. Bishop, B.G. Schuchmann, D.H. Stedman, Environ. Sci. Technol. 47 (2013) 9523–9529.
[5] K. Skalska, J.S. Miller, S. Ledakowicz, Sci. Total Environ. 408 (2010) 3976–3989.
[6] L. Pang, C. Fan, L. Shao, K. Sang, J. Yi, X. Cai, J. Wang, M. Kang, T. Li, Chem. Eng. J. 253 (2014) 394–401.
[7] A. Sultana, M. Sasaki, K. Suzuki, H. Hamada, Catal. Commun. 41 (2013) 21–25.
[8] P.S. Metkar, M.P. Harald, V. Balakotaiah, Appl. Catal. B: Environ. 111–112 (2012) 67–80.
[9] L.J. Xie, F.D. Liu, L.M. Ren, X.Y. Shi, F.S. Xiao, H. He, Environ. Sci. Technol. 48 (2014) 566–572.
[10] N. Wieken, K. Wijayanti, K. Kamasamudran, N.W. Currier, R. Vedojyan, A. Yezerets, L. Olsson, Appl. Catal. B: Environ. 111–112 (2012) 58–66.
[11] J.H. Li, H.Z. Chang, L. Ma, J.M. Hao, R.T. Yang, Catal. Today 175 (2011) 147–156.
[12] X.F. Yang, Z.L. Wu, M. Moses-Debusk, D.R. Mullins, S.M. Mohurin, R.A. Geiger, M. Kidder, C.K. Narula, J. Phys. Chem. C 116 (2012) 23322–23331.
[13] Z. Chajar, M. Priruet, H. Praliand, M. Chevrier, C. Gauthier, F. Mathis, Appl. Catal. B: Environ. 4 (1994) 199–211.
[14] B. Guan, R. Zhan, H. Lin, Z. Huang, Appl. Therm. Eng. 66 (2014) 395–414.
[15] M.P. Ruggeri, I. Nova, E. Tronconi, Chem. Eng. J. 207–208 (2012) 57–65.
[16] M. Koebel, M. Elsener, O. Kröcher, Ch. Schar, R. Rothlisberger, F. Jaussi, M. Mangold, Top. Catal. 30–31 (2004) 43–48.
[17] G. Madia, M. Elsener, M. Koebel, F. Raimondi, A. Wokaun, Appl. Catal. B: Environ. 39 (2002) 181–190.
[18] www.epa.gov/otaq/standards/nonroad/nonroadci.htm consulted on October 29th, (2014).
[19] M. Casanova, K. Schermanz, J. Llorca, A. Trovarelli, Catal. Today 184 (2012) 227–236.
[20] D.M. Chapman, Appl. Catal. A: Gen. 392 (2011) 143–150.
[21] Z.G. Liu, N.A. Ottinger, C.M. Cremeens, Atmos. Environ. 104 (2015) 154–161.
[22] M.A.L. Vargas, M. Casanova, A. Trovarelli, G. Busca, Appl. Catal. B: Environ. 75 (2007) 303–311.
[23] F. Liu, H. He, Z. Lian, W. Shan, L. Xie, K. Asakura, W. Yang, H. Deng, J. Catal. 307 (2013) 340–351.
[24] A. Sagar, A. Trovarelli, M. Casanova, K. Schermanz, SAE Int. J. Engines 4 (2011) 1839–1849.
[25] G. Wu, J. Li, Z. Fang, L. Lan, R. Wang, T. Lin, M. Gong, Y. Chen, Chem. Eng. J. 271 (2015) 1–13.
[26] M. Casanova, J. Llorca, A. Sagar, K. Schermanz, A. Trovarelli, Catal. Today 241 (2015) 159–168.
[27] S. Gupta, Y.P. Yadova, R.A. Singh, J. Mater. Sci. Lett. 5 (1986) 736–738.
[28] M. Bosacka, A. Worsztynowicz, S.M. Kaczmarek, P. Jakubus, J. Phys. Chem. Solids 68 (2007) 1184–1192.
[29] P.I. Cowin, R. Lan, L. Zhang, C.T.G. Petit, A. Kraft, S. Tao, Mater. Chem. Phys. 126 (2011) 614–618.
[30] B. Robertson, E. Kostiner, J. Solid State Chem. 4 (1972) 29–37.
[31] H. Mehner, W. Meisel, A. Brückner, A. York, Hyperfine Interact. 111 (1998) 51–56.
[32] N.N. Greenwood, T.C. Gibb, Mössbauer Spectroscopy, Chapman and Hall Ltd., 1971.
[33] L.J. Alemany, L. Lietti, N. Ferlazzo, P. Forzatti, G. Busca, E. Giamello, F. Bregani, J. Catal. 155 (1995) 117–130.
[34] I. Giakoumelou, C. Fountzoula, C. Kordulis, S. Boghosian, J. Catal. 239 (2006) 1–12.
[35] R. Bharati, R.A. Singh, J. Mater. Sci. 16 (1981) 511–514.
[36] R.Y. Saleh, I.E. Wachs, S.S. Chan, C.C. Chersich, J. Catal. 98 (1986) 102–114.
[37] G. Olivieri, G. Ramis, G. Busca, V. Sanchez Escribano, J. Mater. Chem. 3 (1993) 1239–1249.
[38] K. Routray, W. Zhou, C.J. Kiely, I.E. Wachs, ACS Catal. 1 (2011) 54–66.
[39] A. Löfberg, T. Giornelli, S. Paul, E. Bordes-Richard, Appl. Catal. A: Gen. 391 (2011) 43–51.